Presented in the 5th Hellenic Finance and Accounting Association Conference (HFAA). Thessaloniki, Greece (2006).

Wavelet Analysis and Weather Derivatives Pricing

Achilleas Zapranis[1], Antonis Alexandridis[2]

Abstract. In this paper, we use wavelet analysis to localize in Paris, France, a mean-reverting Ornstein-Uhlenbeck process with seasonality in the level and volatility. Wavelet analysis is an extension of the Fourier transform, which is very well suited to the analysis of non-stationary signals. We use wavelet analysis to identify the seasonality component in the temperature process as well as in the volatility of the temperature anomalies (residuals). Our model is validated on more than 100 years of data collected from Paris, one of the European cities traded at Chicago Mercantile Exchange. We also study the effect of replacing the original AR(1) process with ARMA, ARFIMA and ARFIMA-FIGARCH models, and the impact of the temperature outliers on the normality of the temperature anomalies.

Keywords: Weather Derivatives, Wavelet Analysis, Temperature Dynamic Modeling, AR, ARMA, ARFIMA, FIGARCH, CAT Options, Discrete Pricing Models.

JEL Classification: C51, G13, Q54

[1] Corresponding Author: Assistant Professor, Department of Accounting and Finance, University of Macedonia, 156 Egnatia St., 54006 Thessaloniki, Greece (email: zapranis@uom.gr).
[2] PhD Candidate, Department of Accounting and Finance, University of Macedonia, 156 Egnatia St., 54006 Thessaloniki, Greece (email: aalex@uom.gr).

1. Introduction

Since their inception in 1996, weather derivatives have known a substantial growth. The first parties to arrange for, and issue weather derivatives in 1996, were energy companies, which after the deregulation of energy markets were exposed to weather risk. In September 1999, the Chicago Mercantile Exchange (CME) launched the first exchange traded weather derivatives. In 2004, the notional value of CME weather derivatives was $2.2 billion and grew nine-fold to $22 billion through September 2005, with open interest exceeding 300,000 and volume surpassing 630,000 contracts traded. However, the Over-The-Counter (OTC) market is still more active than the exchange, so the bid-ask spreads are quite large. Today, weather derivatives are being used for hedging purposes by companies and industries, whose profits can be adversely affected by unseasonal weather or, for speculative purposes by hedge funds and others interested in capitalizing on those volatile markets.

A weather derivative is a financial instrument that has a payoff derived from variables such as temperature, snowfall, humidity and rainfall. However, it is estimated that 98-99% of the weather derivatives now traded are based on temperature. This is not surprising since, it is estimated that 30% of the US economy is affected by temperature (CME, 2005). The electricity sector is especially sensitive to the temperature. According to Li and Sailor (1995) and Sailor and Munoz (1997), temperature is the most significant weather factor explaining electricity and gas demand in the United States. The impact of temperature in both electricity demand and price has been considered in many papers, including Henley and Peirson (1998), Peirson and Henley (1994) and Engle *et al* (1992). Unlike insurance and catastrophe-linked instruments, which cover high-risk and low probability events, weather derivatives shield revenues against low-risk and high probability events (e.g., mild or cold winters).

Temperature contracts have as an underlying variable, temperature indices such as Heating Degree Days (HDD) or Cooling Degree Days (CDD) defined on average daily temperatures. A HDD is the number of degrees by which daily temperature is below a base temperature, while a CDD is the number of degrees by which the daily temperature is above the base temperature, i.e., Daily HDD = max (0, base temperature – daily average temperature), Daily CDD = max (0, daily average temperature – base temperature). The base temperature is usually 65 degrees Fahrenheit in the US and 18 degrees Celsius in Europe and Japan. HDDs and CDDs are usually accumulated over a month or over a season. To calculate then we simply add up their daily values for that period.

The list of traded contracts is extensive and constantly evolving. In Europe, CME weather contracts for the summer months are based on an index of Cumulative Average Temperature (CAT). At the end of 2005, at CME were traded weather derivatives for 18 US cities[3], 9 European cities[4], 2 Japanese cities[5], as well as seasonal strip and frost contracts.

[3] Atlanta, Baltimore, Boston, Chicago, Cincinnati, Dallas, Des Moines, Detroit, Houston, Kansas City, Las Vegas, Minneapolis-St. Paul, New York, Philadelphia, Portland, Sacramento, Salt Lake City, Tuscon.
[4] Amsterdam, Barcelona, Berlin, Essen, London, Madrid, Paris, Rome, Stockholm.
[5] Tokyo, Osaka.

Weather risk is unique in that it is highly localized, and despite great advances in meteorological science, still cannot be predicted precisely and consistently. Weather derivatives are also different than other financial derivatives in that the underlying weather index (HDD, CDD,CAT, etc.) cannot be traded. Furthermore, the corresponding market is relatively illiquid. Consequently, since weather derivatives cannot be cost-efficiently replicated with other weather derivatives, arbitrage pricing cannot directly apply to them. The weather derivatives market is a classic incomplete market, because the underlying weather variables are not tradable. When the market is incomplete, prices cannot be derived from the no-arbitrage condition, since it is not possible to replicate the payoff of a given contingent claim by a controlled portfolio of the basic securities. Consequently, the classical Black-Scholes-Merton pricing approach, which is based on no-arbitrage arguments, cannot be directly applied. And market incompleteness is not the only reason for that; weather indices do not follow random walks (as the Black & Scholes approach assumes) and the payoffs of weather derivatives are determined by indices, which are average quantities, whilst the Black-Scholes payoff is determined by the value of the underlying exactly at the maturity date of the contract (European options).

There are several approaches for dealing with incomplete markets. One of them is to introduce the 'market price of risk' for the particular type of the incomplete market, namely a 'factor model', market where there are some non-traded underlying objects. Since, weather derivatives are path depended they are very similar to the average Asian option and similar analytical pricing approaches can be used in this case too. A characteristic example is the approach of Geman and Yor (1993), which used Bessel processes to obtain an exact analytical expression of the Laplace transformation in time of the option price.

A pricing methodology for weather derivatives that is widely used in insurance is the actuarial (or insurance) method. It is based on statistical analysis and it is less applicable in contracts with underlying variables that follow recurrent, predictable patterns. Since, this is the case for most of the weather derivatives contracts, actuarial analysis is not considered the most appropriate pricing approach unless the contract is written on rare weather events such as extreme cold or heat.

Another approach for weather derivatives pricing, is performing simulations based on historical data, known as historical Burn analysis. That is, computing the average payoff of the weather derivatives in the past n years. The central assumption of this method is that the historical record of weather contracts payoffs gives a precise illustration of the distribution of the potential payoffs (Dischel, 1999). If weather risk is calculated as the payoffs standard deviation, then the price of the contract will be $P(t) = D(t, T) \times (\mu \pm \alpha \times \sigma)$, where $D(t, T)$ is the discount factor from contract maturity T to the pricing time t, μ is the historical average payoff, σ is the historical standard deviation of payoffs and a is a positive number denoting risk tolerance. However, since the weather processes are not stationary and this approach does not incorporate forecasts, it is bound to be biased and inaccurate. In fact, the historical Burn analysis is considered as the simplest pricing method in terms of implementation, and the most probable to cause large pricing errors.

In contrast to the previous methods, a dynamic model can be used which directly simulates the future behavior of temperature. Using models for daily temperatures can, in principle, lead to more accurate pricing than modeling temperature indices. In the process of calculating the temperature index, such as HDD, as a normal or lognormal process, a lot of information is

lost (e.g., HDD is bounded be zero). On the other hand, deriving an accurate model for the daily temperature is not a straightforward process. Observed temperatures show seasonality in all of the mean, variance, distribution and autocorrelations and long memory in the autocorrelations. The risk with daily modeling is that small misspecifications in the models can lead to large mispricing in the contracts.

The continuous processes used for modeling daily temperatures usually take a mean-reverting form, which has to descretized in order to estimate its various parameters. Once the process is estimated, one can then value any contingent claim by taking expectation of the discounted future payoff. Given the complex form of the process and the path-dependent nature of most payoffs, the pricing expression usually does not have closed-form solutions. In that case Monte-Carlo simulations are being used. This approach typically involves generating a large number of simulated scenarios of weather indices to determine the possible payoffs of the weather derivative. The fair price of the derivative is then the average of all simulated payoffs, appropriately discounted for the time-value of money; the precision of the Monte-Carlo approach is depended on the correct choice of the temperature process and the look back period of available weather data.

In this paper, we address the problem of pricing the European CAT options. For this purpose we extent the mean-reverting process with seasonality in the level and volatility proposed by Benth and Saltyte-Benth (2005) - a generalisation of (Dornier and Querel, 2000). We incorporate wavelet analysis in the modelling process and we compare the simple AR(1) process with ARMA, ARFIMA and ARFIMA-FIGARCH. The fundamental idea behind wavelets is to analyze according to scale. Wavelet analysis is an extension of the Fourier transform, which superposes sines and cosines to represent other functions. Wavelet analysis decomposes a general function or signal into a series of (orthogonal) basis functions, called wavelets, with different frequency and time locations. The wavelet analysis procedure adopts a particular wavelet function, called a *mother wavelet*. Temporal analysis is performed with a contracted high-frequency version of the mother wavelet, while frequency analysis is performed with a dilated, low-frequency version of the same mother wavelet. Because the original signal can be represented in terms of a wavelet expansion (using coefficients in a linear combination of the wavelet functions), data operations can be performed using just the corresponding wavelet coefficients. A particular feature of the analyzed signal can be identified with the positions of the wavelets into which it is decomposed. Results of the wavelet transform can be presented as a contour map in frequency-time plane (spectrogram), allowing the changing spectral composition of non-stationary signals to be measured and compared. As illustrated in Donoho *et al* (1995) the wavelet approach is very flexible in handling very irregular data series. Ramsey (1999) also comments that wavelet analysis has the ability to represent highly complex structures without knowing the underlying functional form, which is of great benefit in economic and financial research. In order to capture the seasonality of the volatility of the temperature we use a truncated Fourier series. The specific terms of the Fourier series are being selected on the basis of the results of a wavelet analysis of the temperature. As we demonstrate here, wavelet analysis is very useful in offering guidance as to which terms of the Fourier series to select. Our model is validated on more than 100 years of data collected from Paris (from 1900 to 2000), one of the European cities traded at CME.

The rest of the paper is organized as follows. In section 2, we describe the process used to model the average daily temperature in Paris. In section 3, we give an introduction to wavelet

analysis, and examples of its use. In particular, in section 3.1 we compare wavelet analysis to Fourier transform, in section 3.2 we describe wavelets and their use in signal decomposition, in section 3.3 we describe the reverse process of signal reconstruction, in section 3.4 we give an example of analyzing a simulated upward trend with an AR(3) noise component, in section 3.5 we analyze a Geometric Brownian Motion and in section 3.6 we analyze a simulated Ornstein-Uhlenbeck temperature process. Once we have demonstrated, through the examples presented in sections 3.4-3.6, the usefulness of wavelet analysis of temperature processes, we proceed in section 4, were we calibrate the temperature model for Paris. In section 4.1, we perform wavelet analysis of the temperature series. In section 4.2, we estimate and then remove from the temperature the linear trend. In section 4.3, based on the results of the wavelet analysis we model the seasonality component, we estimate it and then we remove it form the temperature. In section 4.4, we model the seasonal residual variance, again using wavelet analysis as a guide in forming the corresponding model. In Section 4.5, we estimate a number of alternative models to the original AR(1) process, i.e., ARMA, ARFIMA, ARFIMA-FIGARCH, and we examine the effect of outlier temperature observations, in order to address the observed deviations from normality. In section 5, we discuss CAT derivatives pricing and finally, in section 6 we conclude.

2. Dynamic Modeling of the Temperature Process

Many different models have been proposed in order to describe the dynamics of a temperature process. The common assumptions in all these models concerning the temperature are the following:

- It follows a predicted cycle.
- It moves around a seasonal mean.
- It is affected by global warming.
- It appears to have autoregressive changes.
- Its volatility is higher in winter than in summer.

Early models were using AR(1) processes or continuous equivalents (Alaton et al, 2002; Davis, 2001; Cao and Wei, 2000). Others like Dornier and Querel (2000) and Moreno (2000) have suggested versions of a more general ARMA(p,q) model. Cabalero *et al* (2002) have shown, however, that all these models fail to capture the slow time decay of the autocorrelations of temperature and hence lead to significant underpricing of weather options. Thus more complex models were proposed, like an Ornstein-Uhlenbeck process (Brody *et al*, 2002). Also in the noise part of the process, the Brownian noise was at first replaced by a fractional Brownian noise and then by a Levy process (Benth and Saltyte-Benth, 2005).

Our analysis will be based on the model of Benth and Saltyte-Benth (2005), where the temperature is expressed as a mean reverting Ornstein-Uhlenbeck process, i.e.

$$dT(t) = dS(t) - \kappa(T(t) - S(t))dt + \sigma(t)dB(t) \quad (1)$$

where, $T(t)$ is the daily average temperature, $B(t)$ is a standard Brownian motion, $S(t)$ is a deterministic function modelling the trend and seasonality of the average temperature, while $\sigma(t)$ is the daily volatility of temperature variations. Benth and Saltyte-Benth (2005) model both $S(t)$ and $\sigma^2(t)$ as a truncated Fourier series:

$$S(t) = a + bt + a_0 + \sum_{i=1}^{I_1} a_i \sin(2i\pi(t - f_i)/365) + \sum_{j=1}^{J_1} b_j \cos(2j\pi(t - g_j)/365) \quad (2)$$

$$\sigma^2(t) = c + \sum_{i=1}^{I_2} c_i \sin(2i\pi t/365) + \sum_{j=1}^{J_2} d_j \cos(2j\pi t/365) \quad (3)$$

From the Ito formula an explicit solution for (1) can be derived:

$$T(t) = s(t) + (T(t-1) - s(t-1))e^{-\kappa t} + \int_{t-1}^{t} \sigma(u)e^{-\kappa(t-u)}dB(u) \quad (4)$$

According to this representation $T(t)$ is normally distributed at t and it is reverting to a mean defined by $S(t)$. The exact specification of models (2) and (3) will be decided based on the results of wavelet analysis of the temperature series.

3. Introduction to Wavelet Analysis: Examples of Its Application to Simulated Time-Series

3.1. Fourier Transform and Wavelet Analysis

Wavelet analysis is a mathematical tool used in various areas of research. Especially, during the last years wavelets are frequently used in order to analyse time-series, data and images. Time-series are represented by local information such as frequency, duration, intensity and time-position and by global information such as the mean states over different time periods. Both global and local information is needed for a correct analysis of a signal. The Wavelet transform (WT) is a generalization of Fourier and windowed Fourier transforms (FT and WFT).

FT breaks down a signal into a linear combination of constituent sinusoids of different frequencies; hence the FT is decomposition on a frequency by frequency basis. However, in transforming to the frequency domain, time information is lost. When looking at a FT of a signal, it is impossible to tell when a particular event took place. This is a serious drawback if the signal properties change a lot over time, i.e., if they contain nonstationary or transitory characteristics: drift, trends, abrupt changes, and beginnings and ends of events. These characteristics are often the most important part of the signal, and FT is not suited to detecting them.

In order to achieve a sort of compromise between frequency and time, FT was expanded in Windowed Fourier Transform. WFT uses a window across the time series and then uses the FT of the windowed series. This is a decomposition of two parameters, time and frequency.

However, since the window size is fixed with respect to frequency, WFT cannot capture events that appear outside the width of the window. Many signals require a more flexible approach that is one where we can vary the window size to determine more accurately either time or frequency.

Wavelet Transform, on the other hand is localized in both time and frequency and overcomes the fixed time-frequency partitioning. The new time-frequency partition is long in time in low- frequencies and long in frequency in high-frequencies. This means that the WT has good frequency resolution for low-frequency events and good time resolution for high-frequency events. Also, the WT adapts itself to capture features across a wide range of frequencies. Consequently the assumption of stationarity can be avoided.

In addition, wavelets have the ability to decompose a signal or a time-series in different levels. As a result, this decomposition brings out the structure of the underlying signal as well as trends, periodicities, singularities or jumps that cannot be observed originally. Wavelets can prove to be a valuable tool for analyzing a wide range of time-series and they have already been used with success in image processing, signal de-noising, density estimation, signal and image compression and time-scale decomposition. Wavelet techniques are being used in finance, for detecting the properties of quick variation of values.

3.2. Wavelets

A wavelet is a waveform of effectively limited duration that has an average value of zero. A *wavelet family* is a set of orthogonal basis functions generated by dilation and translation of a compactly supported *scaling function*, ϕ (or *father wavelet*), and a *wavelet function*, ψ (or *mother wavelet*). The wavelet family consists of *wavelet children* which are dilated and translated forms of a mother wavelet:

$$\psi_{a,b}(t) = \frac{1}{\sqrt{a}}\psi\left(\frac{t-b}{a}\right) \tag{5}$$

where, *a* is the *scale* or *dilation* parameter and *b* is the *shift* or *translation* parameter. The value of the scale parameter determines the level of stretch or compression of the wavelet. The term $1/\sqrt{a}$ normalizes $\left\|\psi_{a,b}(t)\right\| = 1$. In most cases, we will limit our choice of *a* and *b* values by using a discrete set, because calculating wavelet coefficients at every possible scale is computationally intensive. However, if we choose only a subset of scales and translations based on powers of two (the *dyadic* lattice) then our analysis will be much more efficient and just as accurate. We obtain such an analysis from the Discrete Wavelet Transform (DWT). The wavelet family is taken from a double indexed regular lattice:

$$\left\{\left(a_j, b_k\right) = \left(p^j, kqp^j\right) : j,k \in Z\right\} \tag{6}$$

where the parameters *p* and *q* denote the step sizes of the dilation and the translation parameters. For $p = 2$ and $q = 1$ we have the standard dyadic lattice:

$$\left\{\left(a_j, b_k\right) = \left(2^j, k2^j\right) : j, k \in Z\right\} \tag{7}$$

Thus the scaling function ϕ generates for each $j \in \mathbf{Z}$ the sets $V_j = \text{span}\left\{\phi_{j,k}, k \in \mathbf{Z}\right\}$, where **Z** denotes the set of integers and

$$\phi_{j,k}(t) = 2^{-j/2}\phi\left(2^{-j}t - k\right), \quad j, k \in \mathbf{Z} \tag{8}$$

The basis wavelet functions are usually of the form:

$$\psi_{j,k}(t) = 2^{-j/2}\psi\left(2^{-j}t - k\right), \quad j, k \in \mathbf{Z} \tag{9}$$

It follows from above that there is a sequence $\{h_k\}$ (where h_k is a *scaling filter* associated with the wavelet) such that $\sum |h_k|^2 = 1$ and

$$f(t) = \sqrt{2}\sum_{k=0}^{\infty} h_k f\left(2t - k\right) \tag{10}$$

where ϕ is normalized so that $\int_{-\infty}^{\infty} \phi(t)dt = 1$.

When $\{h_k\}$ is finite, a compactly supported scaling function is the solution to the above *dilation equation*. The wavelet function is defined in terms of the scaling function as:

$$\psi(t) = \sqrt{2}\sum_{k=0}^{\infty} g_k \phi\left(2t - k\right) \tag{11}$$

where $\int_{-\infty}^{\infty} \psi(t)dt = 0$ and $g_k = (-1)^{k+1} h^{1-k}$ is a *wavelet filter*.

Then $W_j = \text{span}\left\{\psi_{j,k}, k \in \mathbf{Z}\right\}$ is the orthogonal complement of V_j in V_{j+1}, $\forall j \in \mathbf{Z}$.

Over the years a substantial number of wavelet functions have been proposed in the literature, i.e., Daubechies, Symlet, Coiflet, Biorthogonal, Meyer, Battle-Lemarie, Morlet, Mexican Hat, etc.

3.3. Signal Reconstruction

Representing a signal as a function $T(t)$, the Continuous Wavelet Transform (CWT) of this function comprises the *wavelet coefficients* $C(a,b)$, which are produced through the convulsion of a mother wavelet function $\psi(t)$ with the analyzed signal $T(t)$:

$$C(a,b) = \int_{-\infty}^{+\infty} T(t)\psi\left(\frac{t-b}{a}\right)dt \tag{12}$$

The wavelet coefficients are localized in time and frequency. We term *approximations* the high scale, low frequency components and *details* the low scale, high frequency components. Given the wavelet coefficients we can perform continuous synthesis of the original signal:

$$T(t) = \frac{1}{K_\psi} \int_{-\infty}^{+\infty} \int_{-\infty}^{+\infty} \frac{1}{a^2} \left[C(a,b) \right] \frac{1}{\sqrt{a}} \psi \left(\frac{t-b}{a} \right) da db \tag{13}$$

The DWT of the signal function comprises the *wavelet coefficients* $C(j,k)$, which are produced through the convulsion of a mother wavelet function $\psi_{j,k}(t)$ with the analyzed signal $T(t)$:

$$C(j,k) = \int_{-\infty}^{+\infty} T(t) \psi_{j,k}(t) dt \tag{14}$$

Thus, the discrete synthesis of the original signal is:

$$T(t) = \sum_{j \in Z} \sum_{k \in Z} C(j,k) \psi_{j,k}(t) \tag{15}$$

At each level j, we build the j-level approximation a_j, or approximation at level j, and a deviation signal called the j-level detail d_j, or detail at level j. We can consider the original signal as the approximation at level 0, denoted by a_0. The words approximation and detail are justified by the fact that a_1 is an approximation of a_0 taking into account the low frequencies of a_0, whereas the detail d_1 corresponds to the high frequency correction. For detailed expositions on the mathematical aspects of wavelets we refer to, for example (Mallat, 1999), (Wojtaszczyk, 1997) and (Daubechies, 1992).

3.4. Analyzing a Simulated Signal: Upward Trend plus an AR(3) Noise Component

So far, wavelets have being used in a variety of applications such as signal de-noising, density estimation, variance-covariance estimation and signal compression. Wavelets are able, as it has already been mentioned, to capture changes and events in time-series that are not directly observable. For example, suppose that the signal $T(t)$ consists of a deterministic underlying component $\varphi(t)$ and a noise part $\varepsilon(t)$:

$$T(t) = \varphi(t) + \varepsilon(t) \tag{16}$$

Wavelets are capable of extracting the underlying signal $\varphi(t)$. The de-noising can be achieved by using the appropriate threshold (Donoho and Johnstone, Minimax estimation via wavelet shrinkage, 1998; Donoho and Johnstone, Ideal spatial adaptation by wavelet shrinkage, 1994) in one of the various available algorithms (such as the hard or soft thresholding or the methods described in Gao (1997) and Breiman (1996).

In this example the signal consists of an upward trend plus a colored noise. The colored noise is produced by an AR(3) process:

FIGURE 1. Simulated time-series which consists of an upward trend plus an AR(3) noise component.

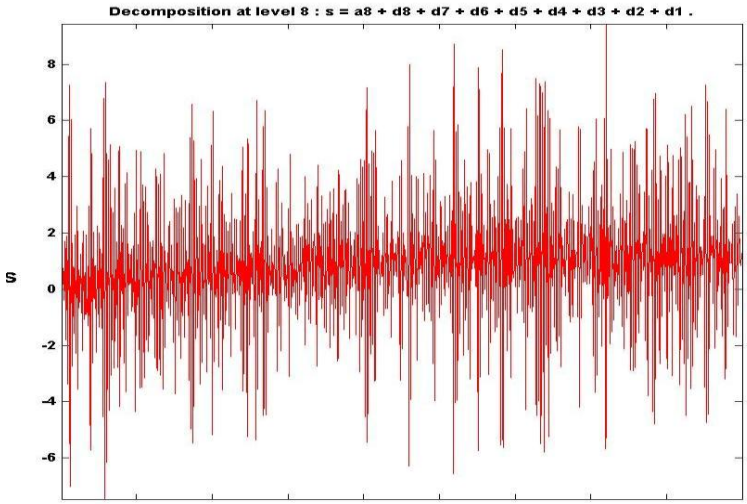

FIGURE 2. Simulated time-series which consists of an upward trend plus an AR(3) noise component and the corresponding denoised signal (solid smooth line).

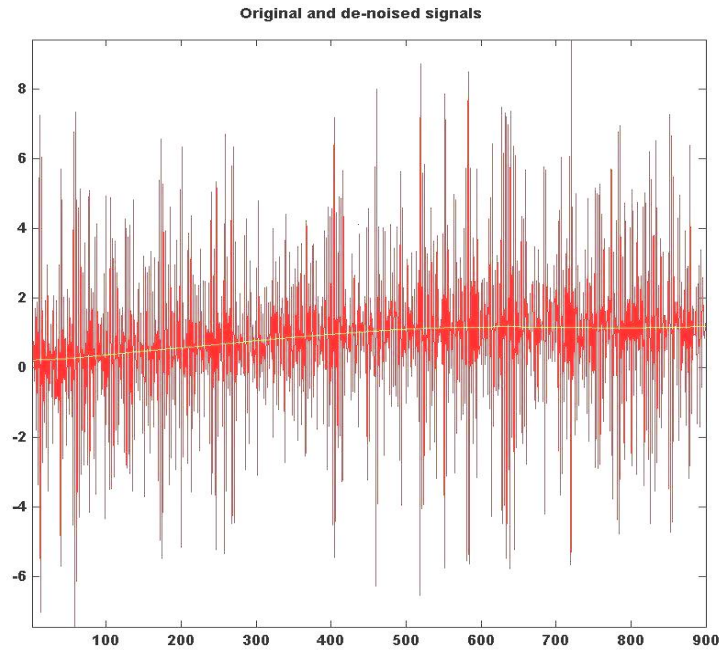

$$z(t) = -1.5z(t-1) - 0.75z(t-2) - 0.125z(t-3) + 0.5 + \varepsilon(t) \tag{17}$$

where $\varepsilon(t)$ are i.i.d. $N(0,1)$.

FIGURE 3. Signal (*s*), approximations (a_j) and details (d_j) of the wavelet decomposition of a simulated time-series which consists of an upward trend plus an AR(3) noise component.

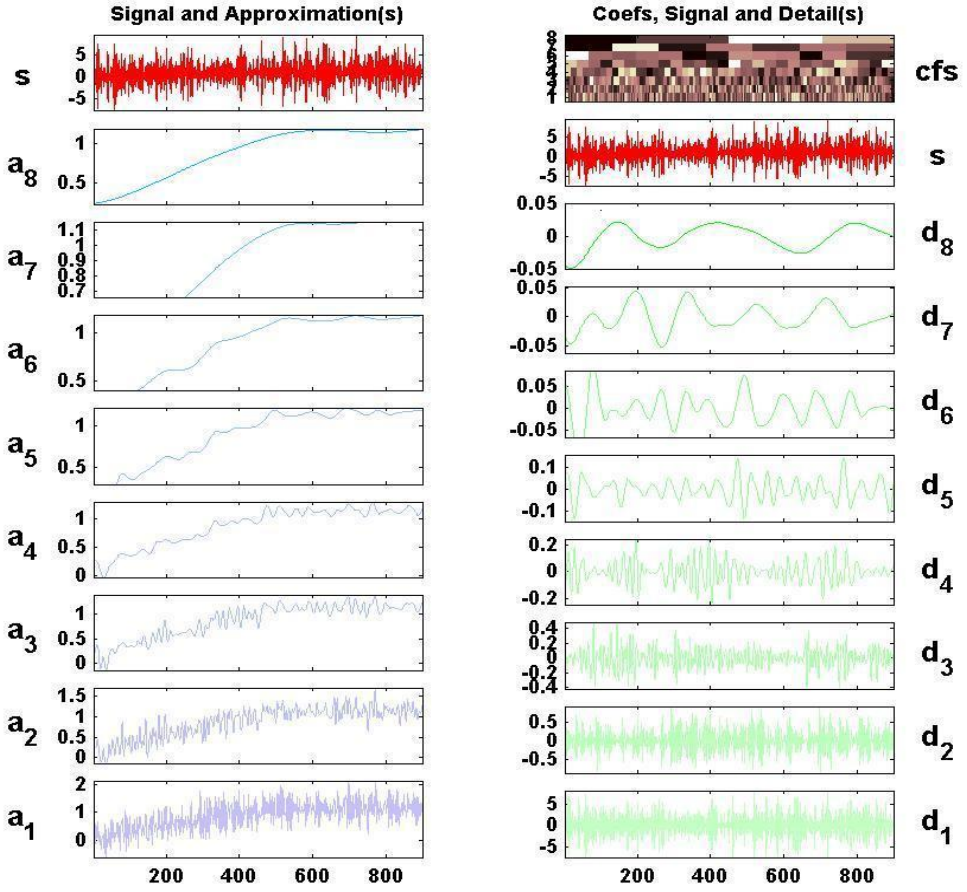

The upward trend is produced by an upward slope, as follows:

$$\varphi(t) = \begin{cases} t/500 + z(t) & \text{t<500} \\ 1 + z(t) & \text{t} \geq 500 \end{cases} \tag{18}$$

As it can be observed in the figure 1, the signal seems like noise. None inference can be drawn for its characteristics.

Wavelets, using the soft thresholding method, succeeded to remove the noise and extract the denoised signal, which is depicted as a solid smooth line in figure 2.

Afterwards, the Daubechies 7 wavelet at level 8 was used in order to decompose the signal. As we can see in figure 3, wavelet transform succeeded to remove the noise starting from the first detail. A good representation of the de-noised signal starts to appear in the third approximation.

FIGURE 4. A geometric Brownian motion (1000 steps) with a jump in volatility at t = 500, where the initial volatility σ_1 = 0.5 doubles to σ_2 = 1.The dotted smooth line represents the exponential upward trend (horizontal axis in thousands).

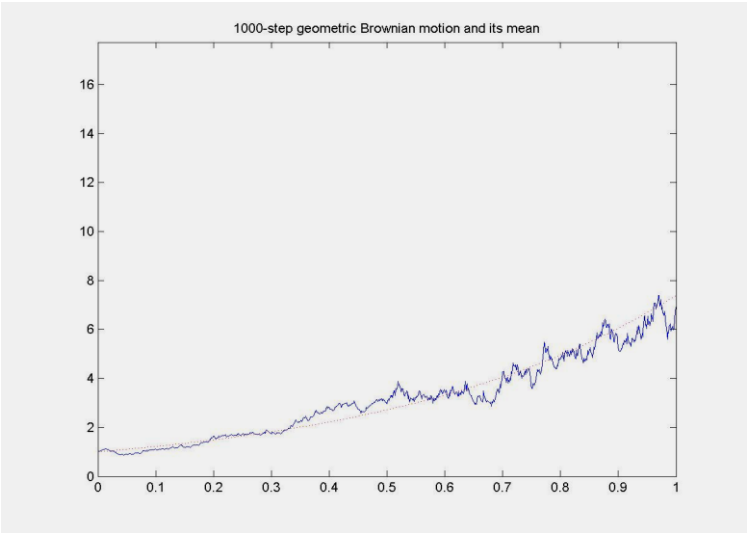

The noise is present in all details, but its effect halves as we move from lower to higher details. Wavelet transform also succeeded in distinguishing the breakpoint with good precision.

3.5. Analyzing a Geometric Brownian Motion

Many financial pricing models are based on the Geometric Brownian Motion. A GBM is produced by the following model:

$$X(t) = X(0)e^{(\mu-\frac{1}{2}\sigma^2)T+\sigma\varepsilon\sqrt{T}} \tag{19}$$

A simple GBM depends on the mean μ and the volatility σ, so it is essential to know whether and when, one or both parameters change. Here we examine, if wavelet analysis can be used to capture changes in the parameters of the GBM model (a simulated path of a GBM process is represented in figure 4).

The volatility of this path changes at t = 500 (0.5) from σ_1 = 0.5 to σ_2 = 1. After applying the Daubechies 8 wavelet at level 8 the decomposition in figure 5 shows clearly the de-noised signal at approximation 8 (a_8), which is the e^x function. The wavelet decomposition also captured the volatility change with a very good precision. In particular, d_1 and d_2 reflect the increase of the random part of the GBM at t = 510, while it actually doubles at t = 500, i.e.,

$$\sigma_2\varepsilon\sqrt{T} = 2\sigma_1\varepsilon\sqrt{T} \tag{20}$$

FIGURE 5. Time-series (s), approximations (a_j) and details (d_j) of the wavelet decomposition, of the wavelet decomposition of a geometric Brownian motion with a jump in volatility.

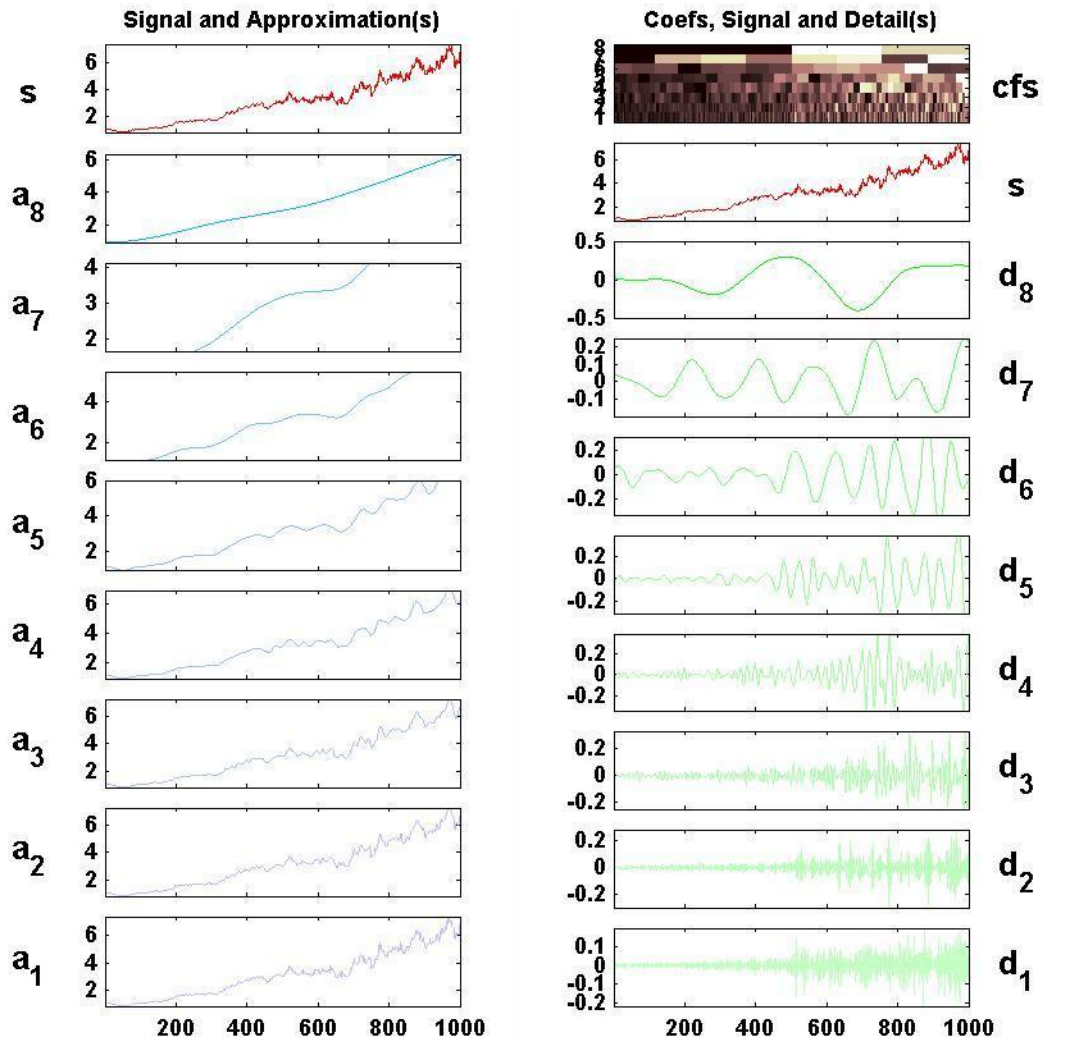

In the next section we examine the wavelet decomposition of an artificial temperature time-series. Climate time series are far more complex than the previous simple examples, since many parameters change both in scales and in time. The following section's simulated temperature time–series includes jumps, singularities, trends, periodicities, as well as model and parameter changes.

3.6. Analyzing a Simulated Ornstein-Uhlenbeck Temperature Process

Lau and Weng (1995) examined the monthly Northern Hemisphere Surface Temperature for the period January 1854 – July 1993 using wavelet analysis. They reported that the temperature has three main frequency branches: inter-annual (2-5 yrs), inter-decadal (10-12 yrs, 20-25yrs and 40-60 yrs) and century (~180 yrs) scales.

By taking into account Lau and Weng's findings, we created an artificial time-series with the properties of a real one, spanning 200 years. We constructed an equation that models the trend and seasonality with their intensity varying across the time horizon.

In doing so, first we needed a component that expresses the global and urban warming. Many papers confirm a linear upward trend during the last years. Hence, we added the linear component $a+bt$ to the last 25 years of the 200 year period.

The temperature on the same date every year is expected to be the same. A sine with period of one year represents the seasonal mean temperature, i.e.,

$\sin(2\pi t / 365)$

Lau *et al.* [16] confirmed seasonalities in the temperature series with a period greater than one year. As a result a cycle with a period of 5 years is present, meaning that every 5 years we have a warm or a cold year, i.e.,

$\sin(2\pi t / (5\cdot 365))$

In addition, we chose the above cycle to disappear for a period of 20 years. In other words, this cycle affects the temperature for the first 95 years, then it disappears for the next 20 years and then it is present again for the last 85 years of the temperature series.

The forth component of the model is a cycle with a 10 year period, which affects the temperature in a different way. Every 10 years the temperature is very high in the summer and very low in the winter or exactly the opposite (low in the summer and high in the winter). This is represented by the following component:

$$\left[1+\sin\left(2\pi t/\left(10\cdot 365\right)\right)\right]\sin\left(2\pi t/365\right)$$

This cycle affects the whole temperature series (200 years). Lastly, we added a cycle that affects the temperature in the same way the 5 year cycle does. However, this cycle's period changes from 40 years to 60 after the first 80 years. This is represented by the following component:

$$\begin{cases}\sin\left(2\pi t/\left(40\cdot 365\right)\right) & \text{t} \le 80 \text{ years}\\ \sin\left(2\pi t/\left(60\cdot 365\right)\right) & \text{t} > 80 \text{ years}\end{cases}$$

After adding all these components the Ornstein-Uhlenbeck temperature process (1) becomes:

$$\begin{aligned}S(t) = a+bt+a_0+a_1\sin\left(2\pi t/365\right)+d_1a_2\sin\left(2\pi t/\left(5\cdot 365\right)\right)+a_3\sin\left(2\pi t/\left(10\cdot 365\right)\right)+\\ +d_2a_4\sin\left(2\pi t/\left(40\cdot 365\right)\right)+d_3a_4\sin\left(2\pi t/\left(60\cdot 365\right)\right)\end{aligned} \quad (21)$$

where

$$d_1\begin{cases}0 & 95 \text{ yrs} \le t \le 115 \text{ yrs}\\ 1 & \text{otherwise}\end{cases} \quad (22)$$

FIGURE 6. Time-series (s), approximations (a_j) and details (d_j) of the wavelet decomposition, of a simulated Ornstein-Uhlenbeck temperature process.

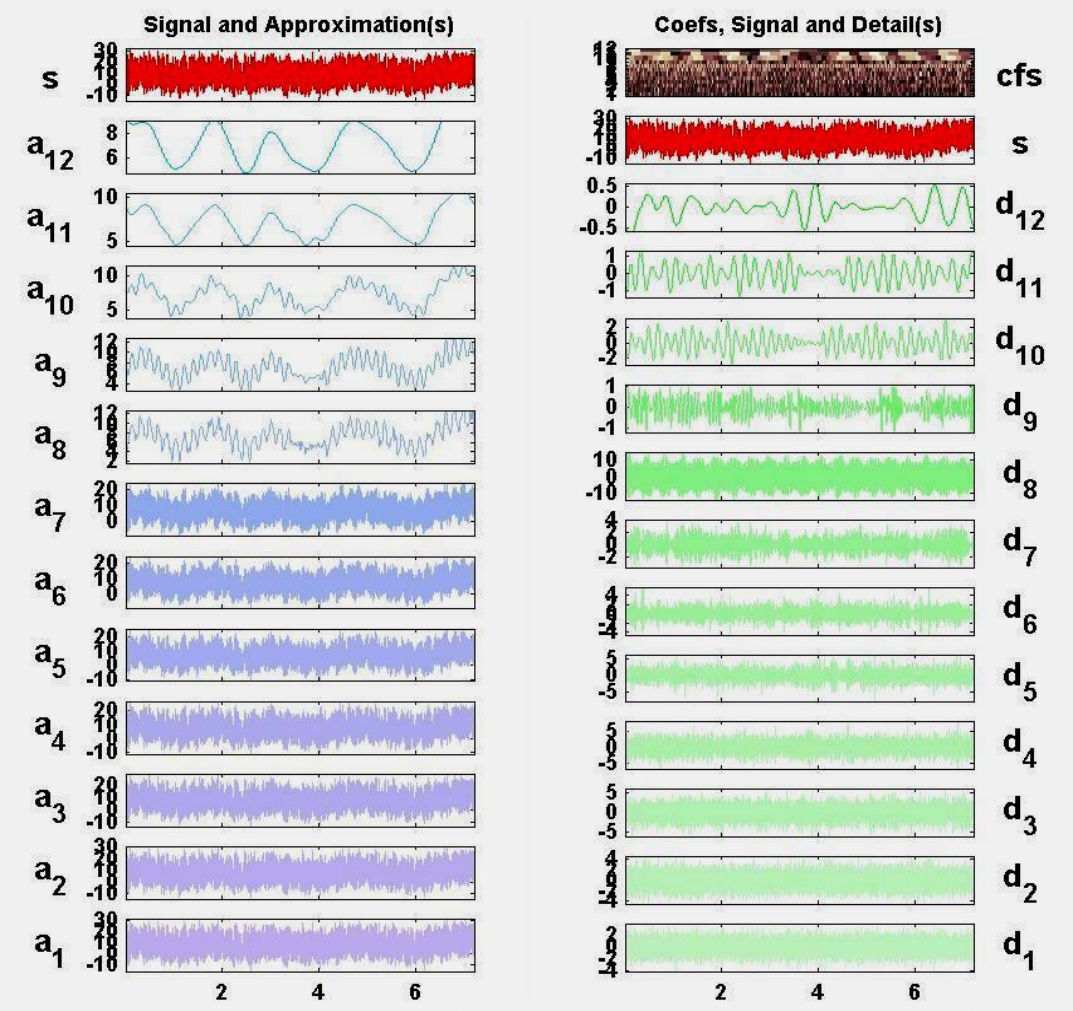

$$d_2 \begin{cases} 1 & t \le 80 \text{ yrs} \\ 0 & \text{otherwise} \end{cases} \tag{23}$$

$$d_3 \begin{cases} 1 & t > 80 \text{ yrs} \\ 0 & \text{otherwise} \end{cases} \tag{24}$$

By substituting 0 by t-1 in equation (4) we get:

$$T(t) = S(t) + \big(T(t-1) - S(t-1)\big)e^{-\kappa} + \int_{t-1}^{t} \sigma(u) e^{-\kappa(t-u)} dB(u) \tag{25}$$

This model was used in order to produce a signal similar to a real temperature time-series. The simulated data consisted of 72,000 values (200 years of daily temperature data). The values of the model parameters are the following:

$a = 0.4$, $b = 0.00002$

$a_0 = 7$, $a_1 = 8$, $a_2 = -2$, $a_3 = 2$, $a_4 = 2$

$k = 0.198$, $t = 200$ years

$I_2 = 4$, $J_2 = 4$

$c = 4$, $c_1 = 0.94$, $c_2 = -0.39$

The Discrete Wavelet Transform was used in order to examine if wavelet analysis can capture all the characteristics of this artificial time-series, such as the upward trend and the four cycles, the properties of these cycles and when these properties are changing.

The decomposition of the artificial time-series was produced by the Daubechies 12 wavelet at level 12 and it is presented in Figure 6. All approximations and details produced by the decomposition are presented here.

The one-year cycle, which is used in the model to express the annual temperature seasonality, is clearly captured in the first seven approximations and in the 8th detail. Approximation a_{12} succeeds in capturing the long cycle of the time-series and its change of period. It is clear, that the period of the signal changes at t = 3. This is reflected by a sine wave whose period at point 29,260 changes from 40 to 60 years. Wavelet decomposition captured perfectly in detail d_8 a product of two sinusoids, with periods of 1 and 10 years, respectively. This product expresses the exact effect that the ten-year cycle has in temperature. Details d_{10} and d_{11} reflect the 5 year seasonal effect. This cycle is inactive for a period of 20 years (95^{th} – 115^{th}). In both d_{10} and d_{11} the starting point of the inactive period is situated with very good approximation at the 97^{th} year. Detail d_{10} also captures correctly the duration of this period, while in d_{11} the inactivity period is significantly larger than 20 years.

The visible upward slope, which appears at the end of each approximation, reflects the upward trend present in the last 25 years of the time-series. Wavelet analysis captures this change in the model approximately at point 62,000 (172 years). Finally, the lower details (d_1 and d_2) reflect the noise part of the time-series.

We repeated the wavelet analysis this time using the Continuous Wavelet Transform. However, since the CWT demands excessive amounts of computer power, even for small datasets, we used monthly average temperatures. The data consisted of 2,400 points. The Mexican hat wavelet function was used. This wavelet usually gives better results than other wavelets using fewer scales. The results of the CWT are presented in Figure 7.

In figure 10 higher scales should represent cycles of long period. Scales higher than 70, capture the long cycle of the time-series and its change of period. This is reflected by a sine wave whose period around the $1,000^{th}$ observation changes from 40 to 60 years. The visible upward slope, that appears at the end of the coefficients line, reflects the upward trend, present in the last 25 years of the time-series. This effect is also visible at Figure 12.

FIGURE 7. Continuous wavelet transform of a simulated Ornstein-Uhlenbeck temperature process.

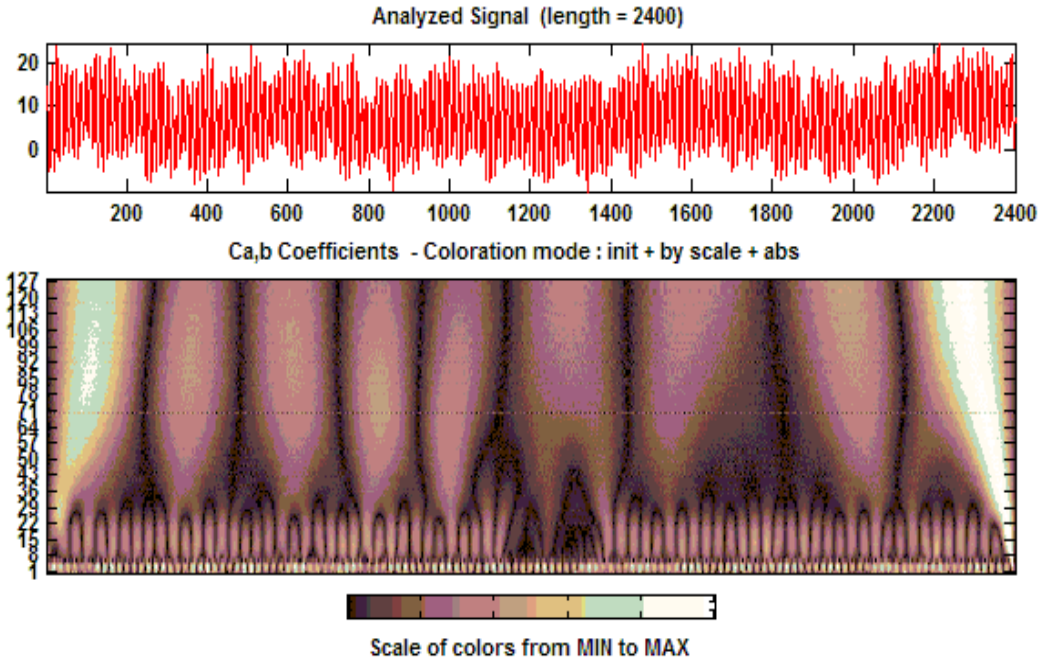

FIGURE 8. Approximations a_{13}, a_4 and a_{11} of the continuous wavelet decomposition, of a simulated Ornstein-Uhlenbeck temperature process.

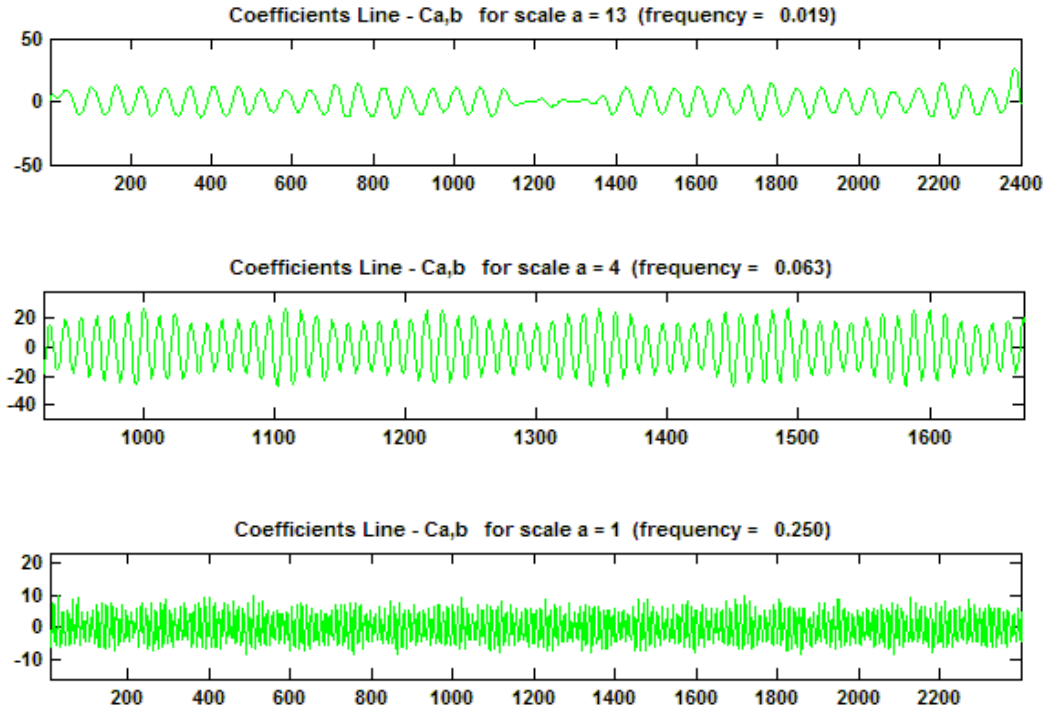

FIGURE 9. Daily average temperature data distribution statistics for Paris, France for the period 1900-2000.

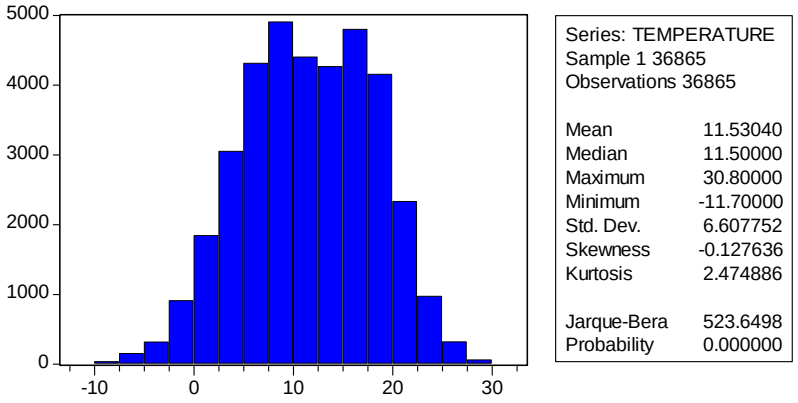

Scales between 8 and 22 reflect the 5 year seasonal effect. This cycle is inactive for a period of 20 years (95^{th} – 115^{th}). In all scales both the starting and ending point of the inactive period is found with very good approximation.

As we can see in Figure 8, the wavelet decomposition captured perfectly in scale between 1 and 8, a product of two sinusoids, with period 1 and 10 years, respectively. This product expresses the exact effect that the ten year cycle has in temperature. Finally, the 1^{st} scale reflects the noise part of the time-series. This scale captures both the effect of the noise and of the ten year cycle.

4. Calibration of Temperature Model

4.1. Wavelet Analysis of Temperature in Paris

In this section real data will be used in order to derive the characteristics and dynamics of temperature. The analysis will be focused in one specific location, i.e., the city of Paris, France. The data consists of 36,865 values, corresponding to the average daily temperatures of 101 years (1900-2000) as measured in the city of Paris. In Figure 9, we can see the descriptive statistics for the data.

For the decomposition of the average daily temperature time-series the Daubechies 11 wavelet at level 11 was used. In Figure 10, we can see all the approximations and details of the decomposed time-series.

FIGURE 10. Daily temperature time-series (s) for Paris, France, approximations (a_j) and details (d_j) produced by the wavelet decomposition.

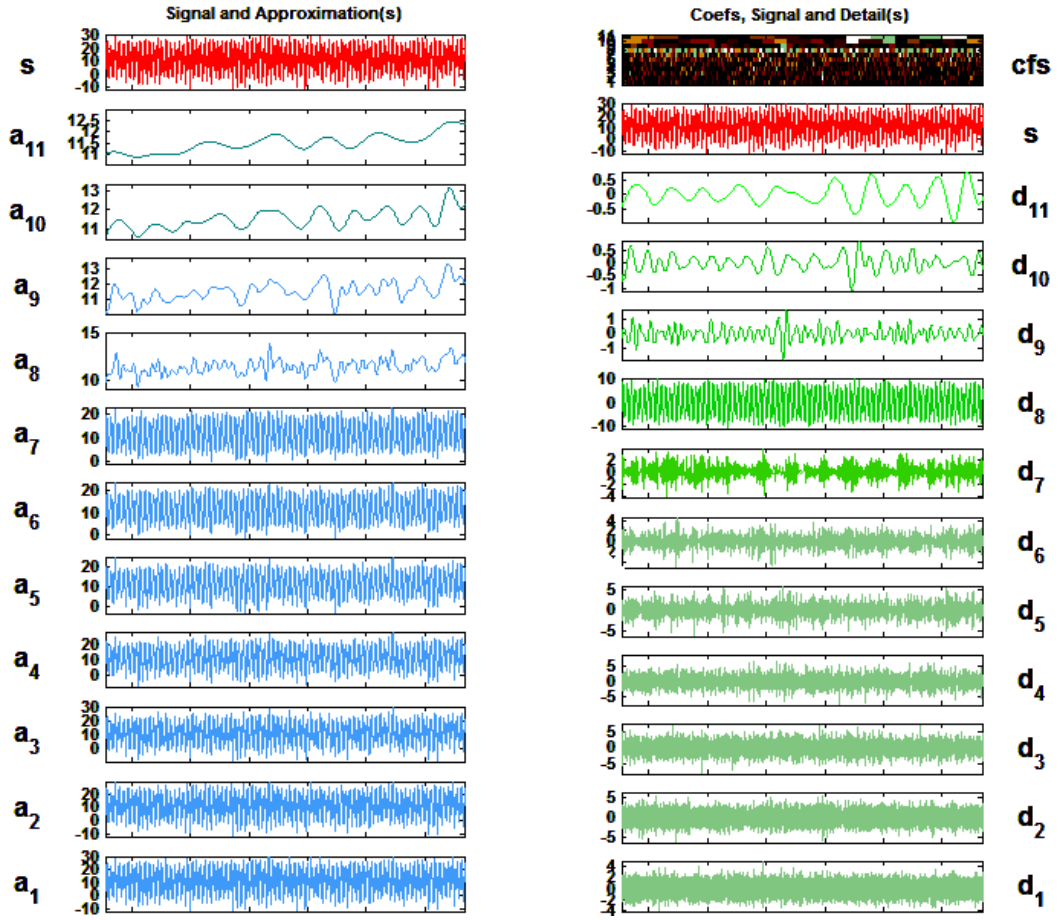

It becomes clear from observing the first seven approximations (a_1 to a_7) and the detail d_8 that there exists a cycle with a period of one year, as it was expected. Approximation a_{11} captures a long cycle with a period of 13 years. Also, in the same approximation an upward trend is observed through the whole period. Detail d_8 also captures a product of two sinusoids, with a period of 1 and 7 years respectively. Details d_{10} and d_{11} reflect a 4-year and an 8-year seasonal effect, respectively. As we can see, both effects are intensive between t = 1-8,000 and t = 20,000-36,865, while the effects between t = 8,000-20,000 are weak. Detail d_9 represents a cycle with period close to 2 years. The visible upward slope, which appears at approximations a_8-a_{11}, reflects the upward trend. The results of wavelet analysis indicate that an upward trend exists throughout the whole period. Finally, the lower details (d_1 and d_2) reflect the noise part of the time-series. A closer inspection of the noise part reveals seasonalities, which will be extracted later on.

FIGURE 11. Fitting a trend to the average daily temperature data in Paris for the period from 1900 to 2000.

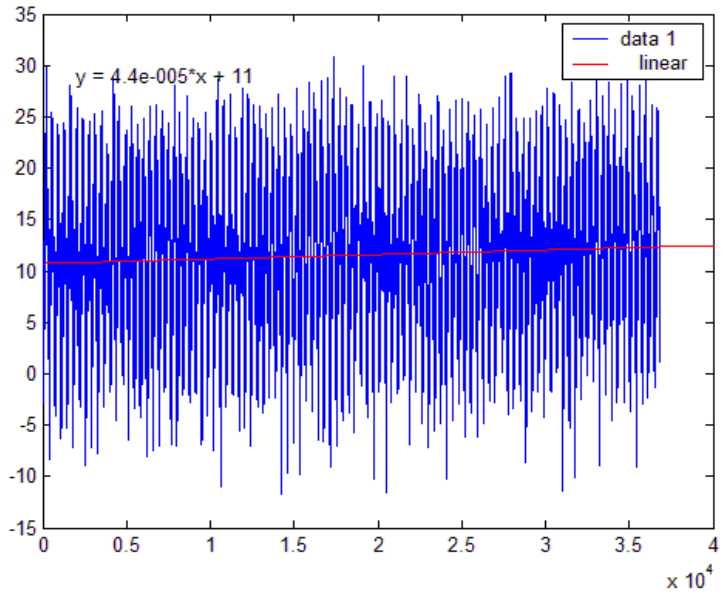

4.2. Estimating the Linear Component

A discrete approximation to the Ito formula (4), which is the solution to the mean reverting Ornstein-Uhlenbeck process (1), is:

$$T(t+1)-T(t)=S(t+1)-S(t)-(1-e^{-k})\{T(t)-S(t)\}+\sigma(t)\{B(t+1)-B(t)\} \quad (26)$$

which can be written as:

$$\tilde{T}(t+1)=a\tilde{T}(t)+\tilde{\sigma}(t)\varepsilon(t) \quad (27)$$

where

$$\tilde{T}(t)=T(t)-S(t) \quad (28)$$

$$\tilde{\sigma}(t)=a\sigma(t) \quad (29)$$

$$a=e^{-k} \quad (30)$$

In order to estimate model (27) we need first to remove the trend and seasonality components from the average temperature series.

Firstly, we quantified the upward trend indicated by the results of the wavelet analysis by fitting a linear regression to the temperature data. The regression was statistically significant with intercept $4.3798 \cdot 10^{-5}$ and slope 10.723. The upward trend is depicted in figure 11. Subtracting the trend form the original data we obtain the de-trended temperature series.

FIGURE 12. The seasonal component of the average daily temperature data in Paris.

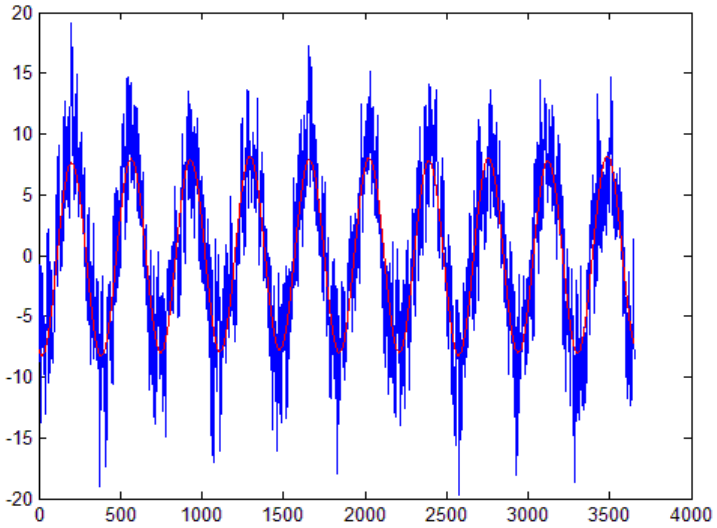

4.3. Estimating the Seasonal Component

The results of the wavelet analysis also indicated that the seasonal part of the temperature takes the following form:

$$\begin{aligned} s_t = {} & a + b_1 \sin(2\pi(t - f_1)/365) + b_2 \sin(2\pi(t - f_2)/(2\cdot 365)) \\ & + b_3 \sin(2\pi(t - f_3)/(13\cdot 365)) + b_4(1+\sin(2\pi(t - f_4)/(7\cdot 365)))\sin(2\pi x/365) \\ & + b_5 \sin(2\pi(t - f_5)/(8\cdot 365)) + b_6 \sin(2\pi(t - f_6/(4\cdot 365)) \end{aligned} \quad (31)$$

The estimated parameters of the above model are given below:

a = -0.0001

b_1 = -8.0214, b_2 = -0.1459, b_3 = -0.1421, b_4 = 0.1741, b_5 = 0.2262, b_6 = -0.0223

f_1 = -71.4571, f_2= 78.09, f_3=-166.1663, f_4 = 787.5860, f_5 = 598.1549, f_6 = 64.5991

Figure 12 depicts the seasonal component of the temperature data for the first 10 years. The mean of the residuals is -1.5887e-008 and the standard deviation of the residuals is 3.4153.

Next we de-seasonalized the temperature series by removing the seasonal component $S(t)$ (see figure 12).

Using the de-trended and de-seasonalized temperature series we estimated the parameters of the model (27), which is an AR(1) process with zero constant. The model statistics are being present in table 1. We observe that the mean reversion parameter a = 0.7978 is statistically significant and that the constant C is very close to zero, as expected. The above value of a corresponds to k = 0.2259 in the original continuous-time dynamics model (1).

TABLE 1. AR(1) model statistics of the de-trended and de-seasonalized Paris average daily data for the period 1900 to 2000.

Variable	Coefficient	St. Error	*t*-statistic	prob.
C	-0.000989	0.053039	0.018650	0.9551
AR(1)	0.797796	0.003140	254.0516	0.0000

R-squared	0.636484	Mean dependent var	-0.000118
Adjusted *R*-squared	0.636475	S.D. dependent var	3.415235
S.E. of regression	2.059150	Akaike info criterion	4.282518
Sum of squared residuals	156298.5	Schwarz criterion	4.282980
Log likelihood	-78933.37	*F*-statistic	64542.19
Durbin-Watson statistic	1.764986	Prob. (*F*-statistic)	0.000000
Inverted AR Roots	.80		

FIGURE 13. Distribution statistics of the residuals of the AR(1) model.

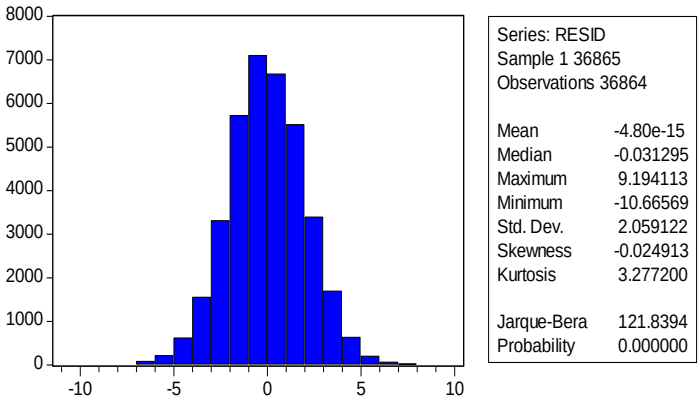

4.4. Modeling the Seasonal Residual Variance

The distributional statistics of the residuals of the AR(1) model, described by equation (27), are given in figure 13. We observe the presence of a negative skewness (-0.024913) and a positive kurtosis (3.277200). From the value of the Jarque-Bera statistic (Bera and Jarque, 1981), i.e., 121.8394, we conclude that there exists a significant deviation from the normal distribution.

FIGURE 14. ACF for the residuals of the AR(1) model of the de-trended and de-seasonalized Paris average daily data.

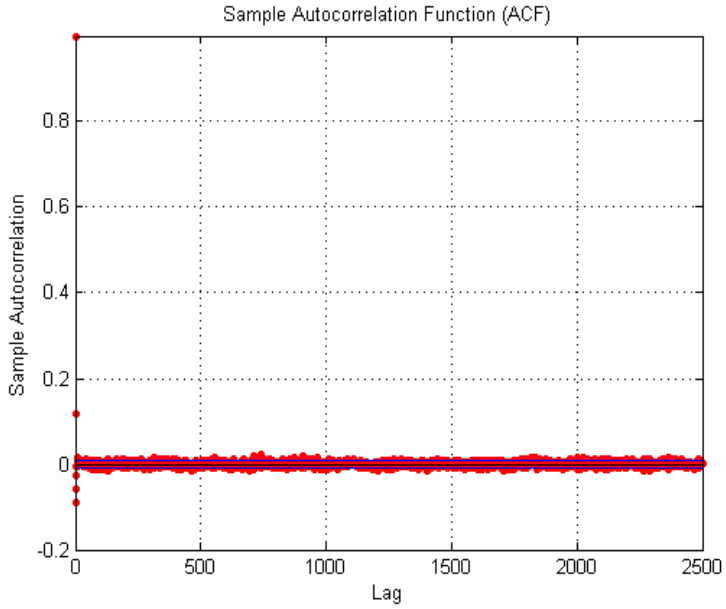

FIGURE 15. ACF of the squared residuals of the AR(1) model of the de-trended and de-seasonalized Paris average daily data.

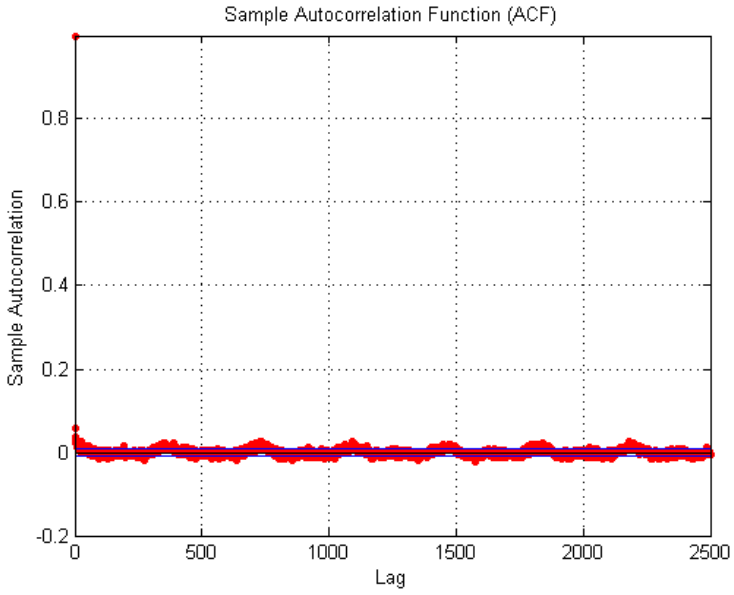

In figures 14 and 15 we can see the autocorrelation functions of the residuals of the AR(1) residuals and of the squared AR(1) residuals, respectively. The autocorrelation of the residuals is significant for the several first lags, while the autocorrelation of the squared residuals indicates a time dependency in the variance of the residuals. In figure 15, we can clearly observe a seasonal variation.

FIGURE 16. Wavelet decomposition of the variance of the residuals $\sigma(t)$.

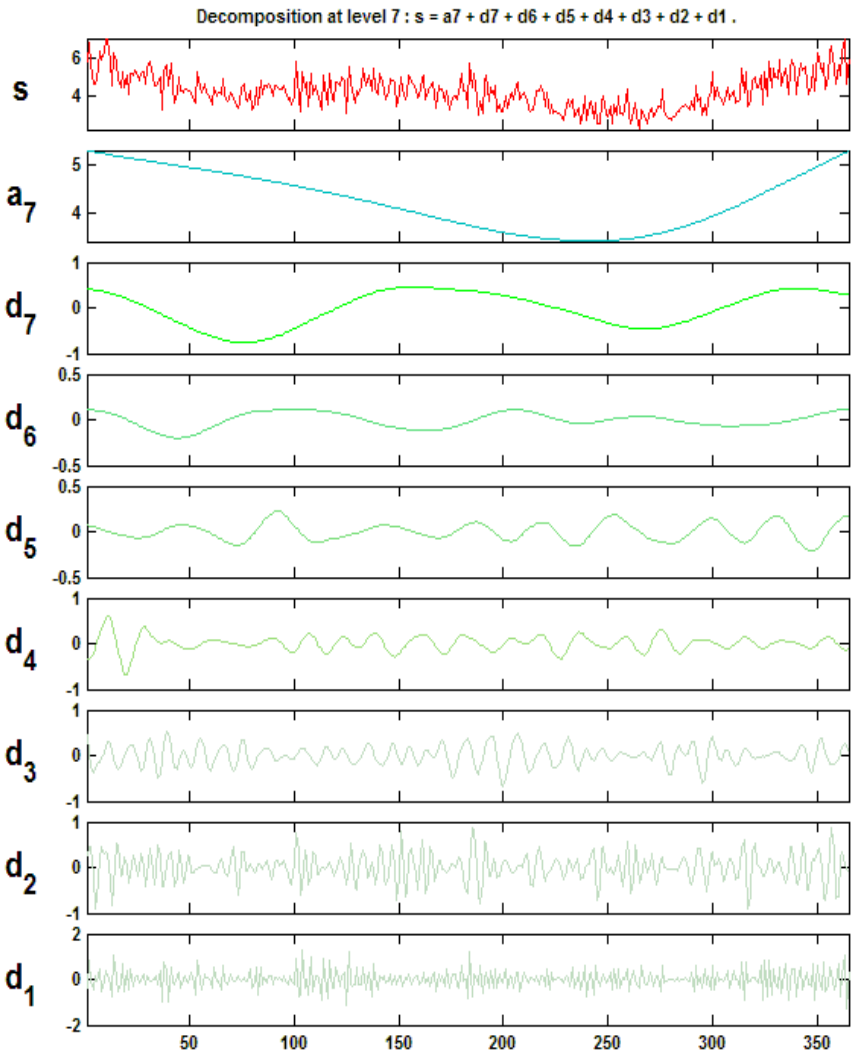

Since, for the residuals $e(t)$ of the AR(1) is true that $e(t) = \tilde{\sigma}^2(t)\varepsilon(t)$, where $\varepsilon(t)$ are i.i.d. $N(0,1)$, we can extract the variance $\tilde{\sigma}^2(t)$ as follows: Firstly, we group the residuals in 365 groups, comprising 101 observations each (each group corresponds to a single day of the year). Then, by taking the average of the squares of each group we obtain $\tilde{\sigma}^2(t)$.

From (29) it is true that:

$$\sigma^2(t) = \frac{\tilde{\sigma}^2(t)}{a^2} \tag{32}$$

where $a = 0.7978$.

FIGURE 17. Empirical variance and fitted variance $\tilde{\sigma}^2(t)$.

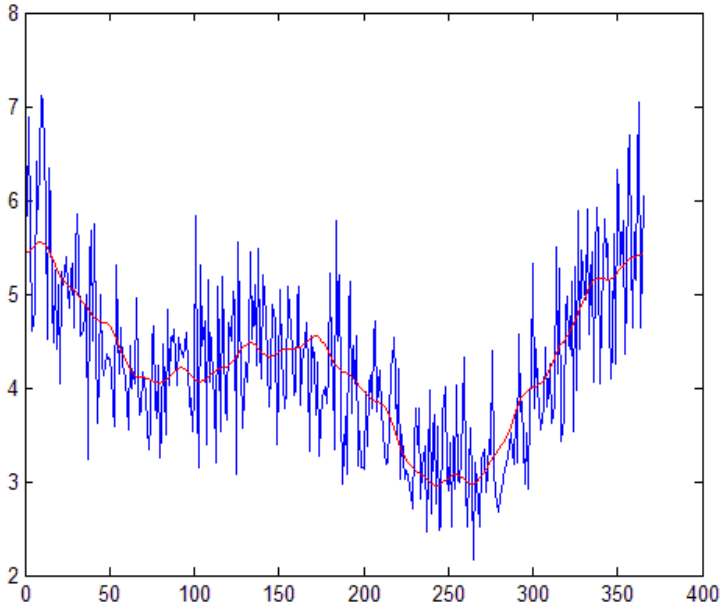

In deciding which terms of a truncated Fourier series to use in order to model the variance $\sigma^2(t)$ (its empirical values are being computed using equation 32), we performed a wavelet analysis. The wavelet decomposition is presented in figure 16. As we can observe from approximation a_7 and details d_4, d_5, d_6, d_7, there exist five cycles within $\sigma^2(t)$. The one-year, the half-year, the 1/4 of a year, the 1/9 of a year and the 1/18 of a year cycles. We model accordingly the variance $\sigma^2(t)$, as follows:

$$\begin{aligned}\sigma^2(t) = {} & c_0 + c_1 \sin(2\pi t/365) + c_2 \sin(4\pi t/365) + \\ & c_3 \sin(8\pi t/365) + c_4 \sin(18\pi t/365) + c_5 \sin(36\pi t/365) + \\ & d_1 \cos(2\pi t/365) + d_2 \cos(4\pi t/365) + \\ & d_3 \cos(8\pi t/365) + d_4 \cos(18\pi t/365) + d_5 \cos(36\pi t/365)\end{aligned} \tag{33}$$

The values of the estimated parameters of model (33) are:

c_0 = 4.2398, c_1 = 0.4324, c_2 = -0.2641, c_3 = 0.0557, c_4 = 0.0843, c_5 = -0.0131,

d_1 = 0.5610, d_2 = 0.6195, d_3 = 0.0326, d_4 = 0.0161, d_5 = -0.0421.

The empirical values of the variance of the residuals (365 values) together with the fitted variance $\tilde{\sigma}^2(t) = a^2\sigma^2(t)$, can be seen in figure 17. We observe that the variance takes its highest values during the winter months, while it takes its lowest values during early Autumn.

FIGURE 18. ACF of the squared residuals of the AR(1) model after dividing out the volatility function $\tilde{\sigma}(t)$ from the regression residuals.

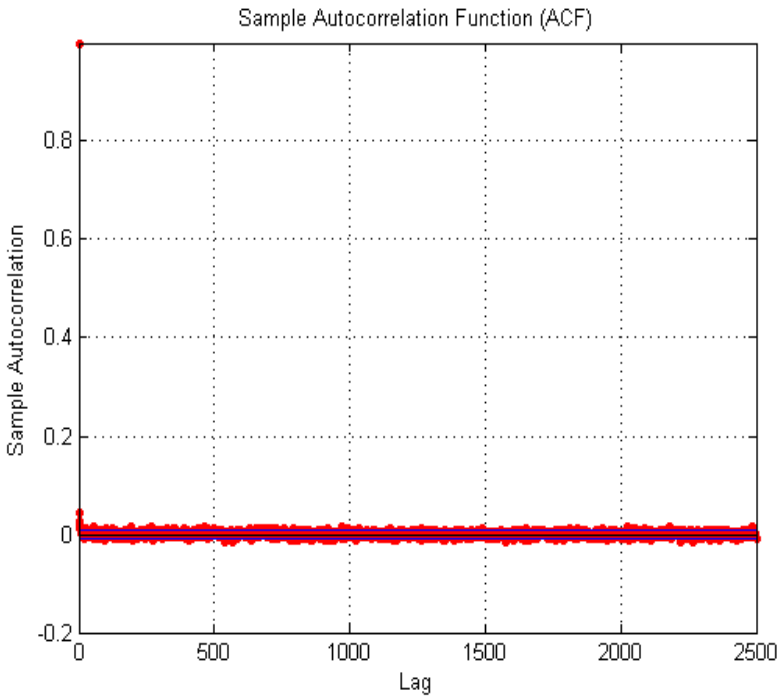

The standard deviation of the residuals is 0.6035, while the standard deviation of the remaining noise part is 1.0003 and its mean is 0.0018. In figure 18, we can see the autocorrelation function of the squared residuals of the AR(1) process after dividing out the volatility function $\tilde{\sigma}(t)$ from the regression residuals. We observe that the seasonality has been removed, but there is still autocorrelation in the first few lags. Moreover, since the Jarque-Bera statistic is 67.6 with a *p*-value of 0.000000, we have to reject the hypothesis of normal distribution.

4.5. Dealing with Non-Normality

The findings of Benth and Saltyte-Benth (2005) for the Copenhagen temperature series are very similar. Although, they did not use wavelet analysis to calibrate their models, they had managed to remove seasonality from the residuals, but their distribution proved to be non-normal. They suggested that a more refined model would probably rectify this problem, but they did not proceed in estimating one. In an earlier paper regarding Norwegian temperature data, Benth and Saltyte-Benth (2004) suggested to model the residuals by a generalized hyperbolic distribution. However, as the same authors comment the inclusion of a non-normal model leads to a complicated Levy process dynamics.

In this paper we eastimated a number of alternatives to the original AR(1) model. In particular we estimated an an ARMA(3,1) model, a long-memory homoscedastic ARFIMA model and a long-memory heteroscedastic ARFIMA-FIGARCH model.

FIGURE 19. Q-Q plot of the residuals of an ARMA(3,1) model.

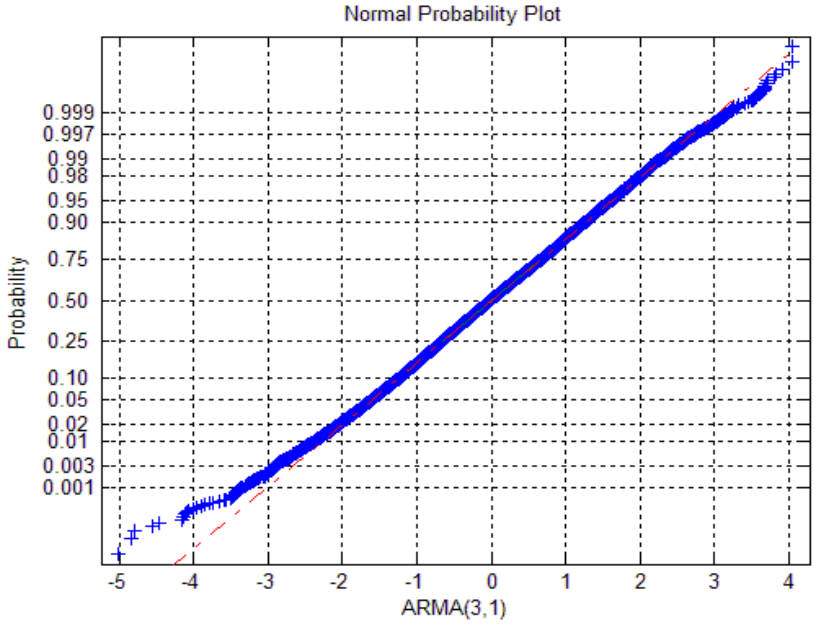

FIGURE 20. Q-Q plot of the residuals of an ARFIMA model.

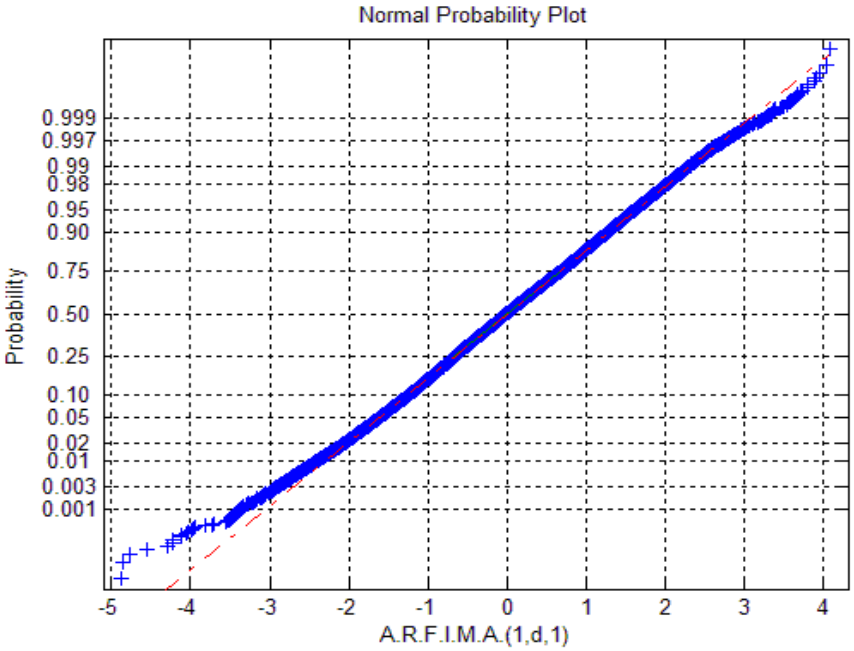

FIGURE 21. Q-Q plot of the residuals of an ARFIMA-FIGARCH model.

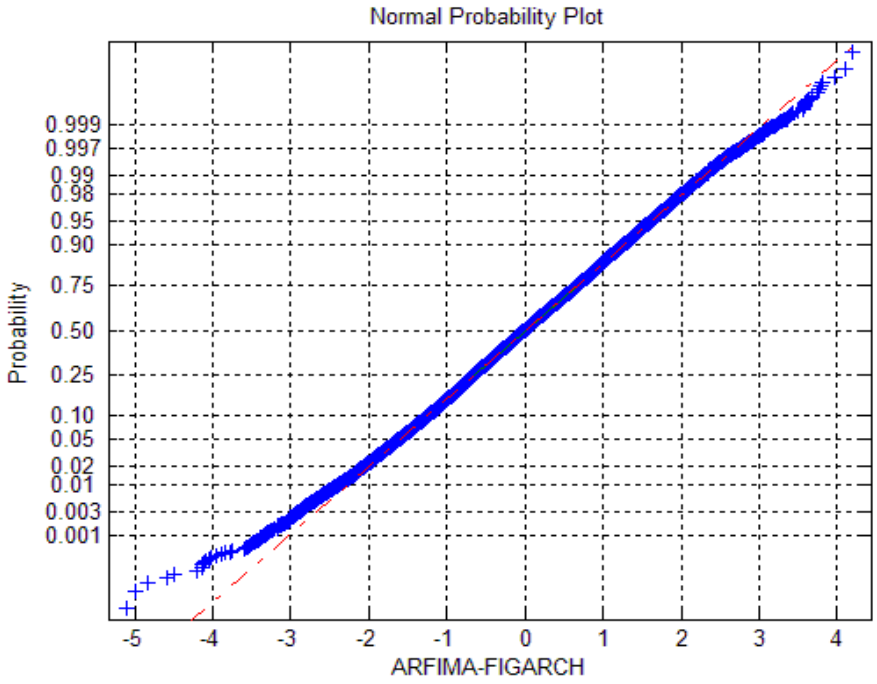

As we can see in the respective Q-Q plots of the residuals in figures 19, 20 and 21 the hypothesis of normality has to be rejected. The Jarque-Bera statistic is above 91 for the ARMA(3,1) model, above 94 for the ARFIMA model and above 114 for the ARFIMA-FIGARCH model. All three models, represent an improvent on our original AR(1) process. Although, the long-memory processes improve the value of the Jarque-Bera statistic, the most appropriate model seems to be the ARMA(3,1) model, which corresponds to the smallest Jarque-Bera statistic.

However, the distribution of the residuals still deviates from normality. The next thing we tried was to assess the impact of outliers to the original AR(1) model. We formed the differences of today's average temperature from yesterday's average temperature and then we identified the dates corresponding to the differences with a value greater than plus or minus 3.5 standard deviations. In total, we identified 40 outlier temperature observations, which were then set equal to the average value of the temperature for that particular day, calculated from 101 years of data. This time the results were surprisingly good. The skewness is -0.005, the kurtosis 3.04 and the Jarque-Bera statistic has fallen to only 3.77.

Concluding, although the AR(1) model probably it is not the best model for describing temperature anomalies, increasing the model complexity (ARMA, ARFIMA, ARFIMA-FIGARCH) and thus the complexity of theoretical derivations in the context of weather derivative pricing does not seem to be justified.

FIGURE 22. Distributional statistics for the residuals of the AR(1) model, after adjusting the outliers to the average temperature for the particular day, calculated from 101 years of data.

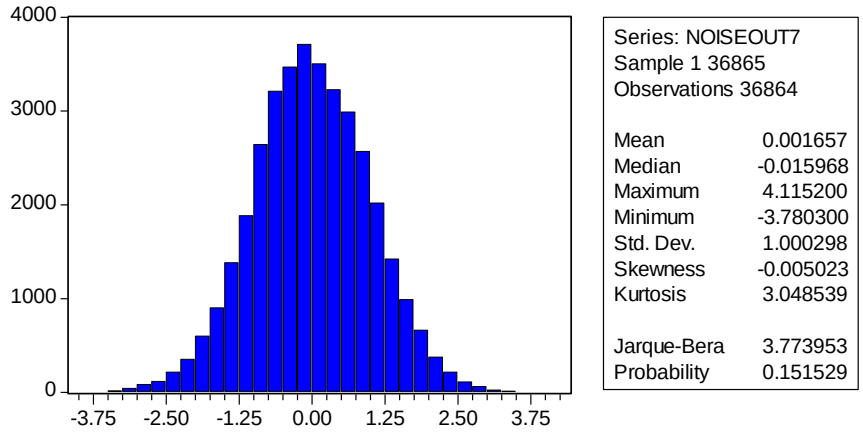

FIGURE 23. Q-Q plot of the residuals of the original AR(1) model and for the AR(1) model after adjusting the outliers to the average temperature for the particular day, calculated from 101 years of data.

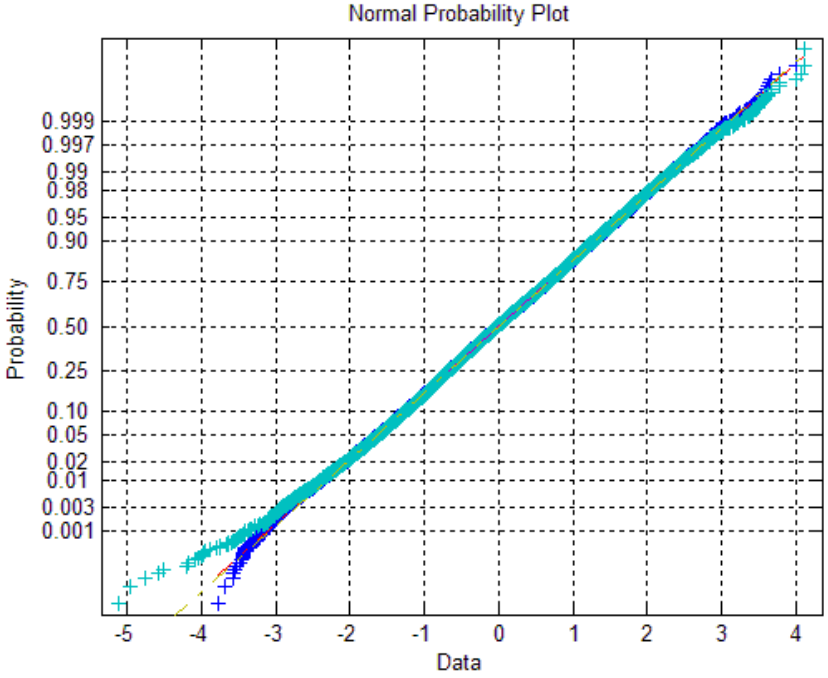

5. Monte-Carlo CAT Derivatives Pricing

The CAT index for time interval $[\tau_1,\tau_2]$ is given by the following expression:

$$\int_{\tau_1}^{\tau_2} \mathrm{T}(\tau)d\tau \tag{34}$$

If Q is the risk neutral probability then the future price of a CAT contract at time t will be:

$$e^{-r(\tau_2-t)}\mathrm{E}_Q\left[\int_{\tau_1}^{\tau_2}\mathrm{T}(\tau)d\tau - F_{CAT}(t,\tau_1,\tau_2)\mid F_t\right]=0 \tag{35}$$

and

$$F_{CAT}(t,\tau_1,\tau_2)=\mathrm{E}_Q\left[\int_{\tau_1}^{\tau_2}\mathrm{T}(\tau)d\tau\mid F_t\right] \tag{36}$$

The stochastic process for the temperature is:

$$dT(t)=ds(t)+\Big(\theta(t)-\kappa\big(T(t)-s(t)\big)\Big)dt+\sigma(t)dW(t) \tag{37}$$

where $\theta(t)$ is a real-valued measurable and bounded function. The solution to this equation is:

$$T(t)=s(t)+\big(T(0)-s(0)\big)e^{-\kappa t}+\int_0^t\theta(u)e^{-\kappa(t-u)}du+\int_0^t\sigma(u)e^{-\kappa(t-u)}dW(u) \tag{38}$$

By replacing this expression to (34) we get:

$$\begin{aligned}\int_{\tau_1}^{\tau_2}\mathrm{T}(\tau)d\tau=&\int_{\tau_1}^{\tau_2}s(t)dt-\kappa^{-1}\big(T(0)-s(0)\big)\left(e^{-\kappa\tau_2}-e^{-\kappa\tau_1}\right)\\&-\int_0^{\tau_2}\theta(t)\kappa^{-1}\left\{e^{-\kappa(\tau_2-t)}-1_{[0,\tau_1]}(t)e^{-\kappa(\tau_1-t)}-1_{[\tau_1,\tau_2]}(t)\right\}dt\\&-\int_0^{\tau_2}\sigma(t)\kappa^{-1}\left\{e^{-\kappa(\tau_2-t)}-1_{[0,\tau_1]}(t)e^{-\kappa(\tau_1-t)}-1_{[\tau_1,\tau_2]}(t)\right\}dW(t)\end{aligned} \tag{39}$$

The future price of a CAT contract $F_{CAT}(t,\tau_1,\tau_2)$ at time $t\le\tau_1$ is:

$$F_{CAT}(t,\tau_1,\tau_2)=\int_{\tau_1}^{\tau_2}s(t)dt-\kappa^{-1}\big(T(t)-s(t)\big)\left(e^{-\kappa(\tau_2-t)}-e^{-\kappa(\tau_1-t)}\right)+\Theta(t,\tau_1,\tau_2) \tag{40}$$

where $\Theta(t,\tau_1,\tau_2)$ is given by the expression:

$$\Theta(t,\tau_1,\tau_2)=\kappa^{-1}\int_t^{\tau_2}\theta(u)\left(1-e^{\kappa(\tau_2-u)}\right)du-\kappa^{-1}\int_t^{\tau_1}\theta(u)\left(1-e^{\kappa(\tau_1-u)}\right)du \tag{41}$$

Since $F_{CAT}(t,\tau_1,\tau_2)$ is an additive Gauss process, we can compute at time t the price of a call option that expires at τ and has strike price K. For $t\le\tau\le\tau_1$ is :

$$C(t)=e^{-r(\tau-t)}(F_{CAT}(t,\tau_1,\tau_2)-\mathrm{K})\Phi(d)+\frac{\Sigma_{t,\tau}}{\sqrt{2\pi}}e^{-d^2/2} \tag{42}$$

where:

$$d=\frac{F_{CAT}(t,\tau_1,\tau_2)-K}{\Sigma_{t,\tau}}$$

$$\Sigma_{t,\tau}^2 := \int_t^\tau \Sigma^2(u, \tau_1, \tau_2) du$$

$$\Sigma(t, \tau_1, \tau_2) := \kappa^{-1}(e^{-\kappa(\tau_1 - t)} - e^{-\kappa(\tau_2 - t)})\sigma(t)$$

6. Conclusions

In this paper, we have used wavelet analysis to identify the seasonality component in the temperature process as well as in the volatility of the residuals, for the average daily temperature in Paris. The temperature anomalies, however, deviated to some extend from normality. To rectify this problem, we estimated a number of alternatives to the original AR(1) model. In particular we estimated an ARMA(3,1) model, a long-memory homoscedastic ARFIMA model and a long-memory heteroscedastic ARFIMA-FIGARCH model. However, none of these alleviated the problem. At list in this case, increasing the model complexity and consequently the complexity of theoretical derivations in the context of weather derivative pricing does not seem to be justified. Next we studied the impact of the temperature outliers. We found that adjusting to average values a small number of outliers resolved the problem, which highlights the importance of pre-processing the temperature data.

References

Alaton, P., Djehinche, B., & Stillberger, D. (2002). On modelling and pricing weather derivatives. *Apllied Mathematical Finance, 9*, 1-20.

Aussem, A., Campbell, J., & Murtagh, F. (1998). Wavelet-based feature extraction and decomposition strategies for financial forecasting. *Journal of Computational Intelligence in Finance, 6* (2), 5-12.

Benth, F. E., & Saltyte-Benth, J. (2004). Stochastic modelling of temperature variations with a view towards weather derivatives. *Applied mathematical Finance*.

Benth, F. E., & Saltyte-Benth, J. (2005). Stochastic modelling of temperature variations with a view towards weather derivatives. *Applied Mathematical Finance, 12* (1), 53-85.

Bera, A. K., & Jarque, C. M. (1981). Efficient tests for normality, homoscedasticity and serial independence of regression residuals: Monte Carlo evidence. *Economics Letters, 7* (4), 313–318.

Breiman, L. (1996). Heuristics of instability and stabilization in model selection. *Annals of Statistics, 24*, 2350-2383.

Brody, C. D., Syroka, J., & Zervos, M. (2002). Dynamical pricing of weather derivatives. *Quantitave Finance, 2*, 189-198.

Cabalero, R., Jewson, S., & Brix, A. (2002). Long memory in surface air temperature: Detection, modeling and application to weather derivatives. *Climate Research, 21*, 127-140.

Cao, M., & Wei, J. (2000). Pricing the weather. *Risk, 13* (5).

CME. (2005). *An Introduction to CME Weather Products.* Retrieved from http://www.cme.com.

Daubechies, I. (1992). *Ten Lectures on Wavelets (CBMS-NSF Regional Conference Series in Applied Mathematics).*

Davis, M. (2001). Pricing weather derivatives by marginal value. *Quantitative Finance, 1*, 305-308.

Dischel, B. (1999, October). Shaping history. *Wether Risk*, 8-9.

Donoho, D. L., & Johnstone, I. M. (1994). Ideal spatial adaptation by wavelet shrinkage. *Biometrika, 81*, 425-455.

Donoho, D. L., & Johnstone, I. M. (1998). Minimax estimation via wavelet shrinkage. *Annals of Statistics, 26*, 879-921.

Dornier, F., & Querel, M. (2000, August). Caution to the wind. *Energy Power Risk Management*, 30-32.

Engle, R. F., Mustafa, C., & Rice, J. (1992). Modeling peak electricity demand. *Journal of forecasting, 11*, 241-251.

Gao, H. Y. (1997). Wavelet shrinkage denoising using non-negative garrotte. *Journal of Computational and Graphical Statistics, 7*, 469-488.

Geman, H., & Yor, M. (1993). Bessel processes, Asian options, and perpetualities. *Mathematical Finance, 3*, 349-375.

Henley, A., & Peirson, J. (1998). Residential energy demand and the interaction of price and temperature: British experimental evidence. *Energy Economics, 20*, 157-171.

Lau, K. M., & Weng, H. Y. (1995). Climate signal detecting using wavelet signal transform. *Bulletin of American Meteorological Society, 76*, 2391-2402.

Li, X., & Sailor, D. J. (1995). Electricity use sensitivity and climate and climate change. *World Resource Review, 3*, 334-346.

Mallat, S. G. (1999). *A wavelet tour of signal processing.* San Diego: Academic Press.

Moreno, M. (2000). Riding the temp. *Futures and Options World, 11*.

Peirson, J., & Henley, A. (1994). Electricity load and temperature issues in dynamic specification. *Energy Economis, 16*, 235-243.

Percival, D. B., & Walden, A. T. (2000). *Wavelet Methods for Time Series Analysis.* Cambridge, England: Cambridge University Press.

Sailor, D. J., & Munoz, R. (1997). Sensitivity of electricity and natural gas consumption to climate in the USA - Meteorology and results for eight States. *Energy the International Journal, 22*, 987-998.

Torrence, C., & Compo, P. G. (1998). A practical guide to wavelet analysis. *Bulletin of American Meteorological Society, 79*, 61-75.

Wojtaszczyk, P. (1997). *A Mathematical Introduction to Wavelets.* Cambridge: Cambridge University Press.